nature genetics

Mutations in dynamin 2 cause dominant centronuclear myopathy

Marc Bitoun[1], Svetlana Maugenre[1], Pierre-Yves Jeannet[2], Emmanuelle Lacène[1], Xavier Ferrer[3], Pascal Laforêt[1], Jean-Jacques Martin[4], Jocelyn Laporte[5], Hanns Lochmüller[6], Alan H Beggs[7], Michel Fardeau[1], Bruno Eymard[1], Norma B Romero[1] & Pascale Guicheney[1]

Autosomal dominant centronuclear myopathy is a rare congenital myopathy characterized by delayed motor milestones and muscular weakness. In 11 families affected by centronuclear myopathy, we identified recurrent and *de novo* missense mutations in the gene dynamin 2 (*DNM2*, 19p13.2), which encodes a protein involved in endocytosis and membrane trafficking, actin assembly and centrosome cohesion. The transfected mutants showed reduced labeling in the centrosome, suggesting that *DNM2* mutations might cause centronuclear myopathy by interfering with centrosome function.

Autosomal dominant centronuclear myopathy (CNM) is a congenital myopathy characterized by slowly progressive muscular weakness and wasting[1]. The disorder involves mainly limb girdle, trunk and neck muscles but may also affect the distal muscles. Weakness may be present during childhood or adolescence or may not become evident until the third decade of life. Some affected individuals become wheelchair-bound in their fifties. Ptosis and limitation of eye movements occur frequently. The most prominent histopathological features include high frequency of centrally located nuclei in a large number of the extrafusal muscle fibers, radial arrangement of sarcoplasmic strands around the central nuclei and predominance and hypotrophy of type 1 fibers[2,3]. The severe X-linked form of CNM, X-linked myotubular myopathy, is caused by mutations in the gene *MTM1*, which encodes myotubularin, a highly conserved phosphoinositide phosphatase probably involved in membrane trafficking[4].

We carried out genome-wide linkage mapping analysis in two families with autosomal dominant CNM (families 1 and 2) with eight and six affected members, respectively (**Supplementary Methods** online). Only three markers, *D19S884*, *D19S865* and *D19S226*, gave positive lod scores in these two families. We confirmed that this locus was linked to CNM by genotyping other affected family members and a third multigenerational family (family 3). We genotyped additional microsatellite markers and identified several recombination events that narrowed the CNM locus on chromosome 19p13.2 to a 11.03-Mb interval between *D19S1034* and *D19S899* (**Supplementary Table 1** and **Supplementary Fig. 1** online).

To identify proteins potentially responsible for the morphological abnormalities observed in CNM, we evaluated candidate proteins using three criteria: (i) expression in skeletal muscle, (ii) involvement in membrane trafficking (myotubularin-like hypothesis) and (iii) direct or indirect involvement in cytoskeleton. This focused our attention on ubiquitous protein dynamin 2 (DNM2), encoded by *DNM2* (ref. 5). Dynamins are large GTPases involved in membrane trafficking that act as mechanochemical scaffolding molecules that can hydrolyze GTP to deform biological membranes[6]. Among the dynamin family, the 100-kDa GTPase DNM2 has roles in endocytosis at the plasma membrane[6], membrane trafficking from the trans-Golgi network[7], formation of actin stress-fibers[8], actin-membrane interface assembly[9] and centrosome cohesion[10].

We sequenced exons and intron-exon boundaries of *DNM2* in the probands of families 1–3 and identified heterozygous missense mutations (**Table 1** and **Supplementary Fig. 2** online). Two were located in exon 8, 1106G→A resulting in the amino acid substitutions R369Q in family 2 and 1105C→T resulting in the amino acid substitution

Table 1 Summary of *DNM2* mutations

Family	Family number	Number of mutation carriers	Origin	Exon	Nucleotide change	Amino acid change
1	3012	9	France	11	1393C→T	R465W
2	11451	14	French Guyana	8	1106G→A	R369Q
3	961	5	France	8	1105C→T	R369W
4	9346	1	France	8	1102G→A	E368K
5	IBB/CNM1	4	Belgium	11	1393C→T	R465W
6	IBB/CNM2	3	Belgium	11	1393C→T	R465W
7	E/CNM3	4	Germany	11	1393C→T	R465W
8	E/393	2	Great Britain	11	1393C→T	R465W
9	E/703	4	US	11	1393C→T	R465W
10	722	1	France	8	1105C→T	R369W
11	14815	3	France	8	1105C→T	R369W

Nucleotide numbers are indicated relative to the first translated base (the A from the ATG initiation codon). All mutations affect CpG dinucleotides. Families 1, 2, 4, 10 and 11 have been thoroughly described[2] (they correspond to families 1, 3, 8, 11 and 2, respectively, in ref. 2). Family 9 from the US is of European origin.

[1]INSERM U582, Institute of Myology, IFR14, Groupe Hospitalier Pitié-Salpêtrière, UPMC, 47 Boulevard de l'Hôpital, 75651 Paris Cedex 13, France. [2]Department of Pediatrics, Neuropediatric Unit, CHUV, Lausanne, Switzerland. [3]Department of Neurology, CHU Haut-Lévêque, Bordeaux, France. [4]Laboratory of Neuropathology, Born-Bunge Institute, Antwerp, Belgium. [5]Department of Molecular Pathology, I.G.B.M.C., CNRS/INSERM/ULP/Collège de France, Illkirch, France. [6]Friedrich Baur Institute, Department of Neurology, Ludwig Maximilians University, Munich, Germany. [7]Genetics Division, Children's Hospital Boston, Harvard Medical School, Boston, USA. Correspondence should be addressed to P.G. (p.guicheney@myologie.chups.jussieu.fr).

Received 22 March; accepted 23 August; published online 16 October 2005; doi:10.1038/ng1657

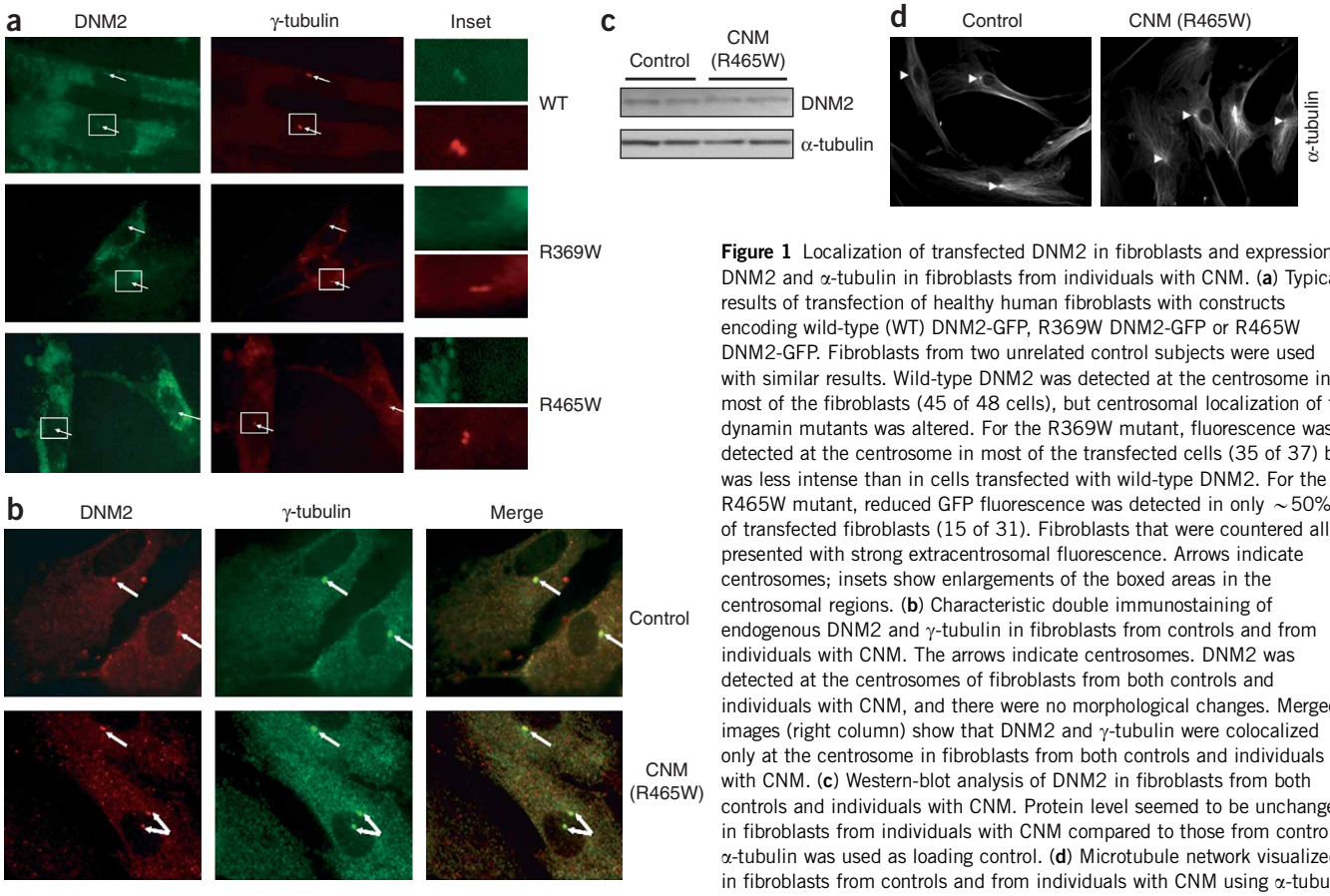

Figure 1 Localization of transfected DNM2 in fibroblasts and expression of DNM2 and α-tubulin in fibroblasts from individuals with CNM. (**a**) Typical results of transfection of healthy human fibroblasts with constructs encoding wild-type (WT) DNM2-GFP, R369W DNM2-GFP or R465W DNM2-GFP. Fibroblasts from two unrelated control subjects were used with similar results. Wild-type DNM2 was detected at the centrosome in most of the fibroblasts (45 of 48 cells), but centrosomal localization of the dynamin mutants was altered. For the R369W mutant, fluorescence was detected at the centrosome in most of the transfected cells (35 of 37) but was less intense than in cells transfected with wild-type DNM2. For the R465W mutant, reduced GFP fluorescence was detected in only ~50% of transfected fibroblasts (15 of 31). Fibroblasts that were countered all presented with strong extracentrosomal fluorescence. Arrows indicate centrosomes; insets show enlargements of the boxed areas in the centrosomal regions. (**b**) Characteristic double immunostaining of endogenous DNM2 and γ-tubulin in fibroblasts from controls and from individuals with CNM. The arrows indicate centrosomes. DNM2 was detected at the centrosomes of fibroblasts from both controls and individuals with CNM, and there were no morphological changes. Merged images (right column) show that DNM2 and γ-tubulin were colocalized only at the centrosome in fibroblasts from both controls and individuals with CNM. (**c**) Western-blot analysis of DNM2 in fibroblasts from both controls and individuals with CNM. Protein level seemed to be unchanged in fibroblasts from individuals with CNM compared to those from controls. α-tubulin was used as loading control. (**d**) Microtubule network visualized in fibroblasts from controls and from individuals with CNM using α-tubulin immunostaining. The arrowheads show the microtubule organizing centers. There was no apparent disorganization of microtubule network in fibroblasts from individuals with CNM.

R369W in family 3. In family 1, a mutation in exon 11 (1395C→T) resulted in the amino acid substitution R465W. We also identified missense mutations in eight additional families with either dominant inheritance or sporadic cases of CNM. The R465W mutation was present in five additional families and the R369Q mutation in two others (**Table 1**). Genotyping of SNPs surrounding the R369Q and R465W mutations uncovered several genetic backgrounds among individuals sharing the same mutation (data not shown). We identified a new missense mutation, 1102G→A, resulting in the amino acid substitution E368K, in the proband of family 4, which was not found in the parents. We confirmed paternity of the proband and therefore concluded that the mutation occurred *de novo*. The R369W mutation in family 3 was also probably a *de novo* event (**Supplementary Fig. 1**). All the mutations cosegregated with the disease in the 11 families and were not found in 150 healthy control subjects of European descent screened by single strand conformation polymorphism analysis (for mutations R465W and E368K) or restriction enzyme digestion using *Aci*I (for mutations R369W and R369Q, because single strand conformation polymorphism profiles were not informative for these mutations; **Supplementary Fig. 2**). Taken together, our results suggest that *DNM2* mutations cause CNM. The severity of disease in affected individuals carrying one of the two most frequent mutations did not differ greatly, but disease onset occurred earlier in some individuals carrying the R465W mutation compared with those carrying the R369Q mutation. This observation needs to be confirmed in a larger sample of individuals.

The three mammalian dynamins share the same protein structure (**Supplementary Fig. 3** online), with an N-terminal tripartite GTPase domain, a middle domain, a pleckstrin homology domain, a GTPase effector domain and a C-terminal proline rich domain. DNM2 mutations restricted to the pleckstrin homology domain, which mediates interaction with phosphoinositides, were recently identified in the dominant intermediate form of Charcot-Marie-Tooth disease type B[11]. In CNM, the four mutations, affecting three highly conserved residues (**Supplementary Fig. 3**), were all restricted to the middle domain. The middle domain is involved in self-assembly of the molecule[12], and the GTPase activity induces a conformational change of this domain associated with a constriction of lipidic structures[13]. Moreover, the middle domain is essential for the centrosomal localization of DNM2 (ref. 10).

To explore the capability of DNM2 mutants to localize to the centrosome, we prepared green fluorescent protein (GFP) chimeras using wild-type, R369W and R465W DNM2 constructs. Wild-type DNM2-GFP was detected in the centrosome in transfected human fibroblasts. In contrast, the fluorescence associated with the centrosome was markedly reduced in the fibroblasts transfected with mutant DNM2-GFP constructs and was almost absent in roughly one-half of the fibroblasts transfected with R465W DNM2 (**Fig. 1a**). In addition, we observed similar levels of DNM2 in fibroblasts from controls and from individuals with CNM carrying the R465W mutations, as measured by both cell immunolabeling and western blotting (**Fig. 1b,c**), suggesting that the mutant protein was relatively stable.

On the basis of these results, we hypothesize that mutations might hinder either the transport of DNM2 to the centrosome or its interaction with some centrosomal components, such as γ-tubulin[10]. Such phenomena might be responsible for a defect in a centrosomal function through a dominant negative effect. Nevertheless, we cannot exclude that the mutations associated with CNM might also alter other mechanisms that involve the DNM2 middle domain.

Furthermore, immunohistochemical analysis with polyclonal DNM2 antibody on muscle biopsy samples from five affected individuals and four controls showed no differences in labeling intensity, despite some mild changes in labeling distribution, which were probably due to the particular rearrangement of the intermyofibrillar network (data not shown). In addition, the microtubular network visualized by α-tubulin labeling appeared correctly organized in fibroblasts from individuals with CNM (**Fig. 1d**). Even if microtubule nucleation is probably not impaired in fibroblasts from individuals with CNM, the situation could differ in skeletal muscle; during differentiation, centrosomes disappear and the microtubule-organizing center is redistributed near the nuclear membrane and in some new cytoplasmic sites of nucleation[14]. Concurrently, the microtubular network is rearranged longitudinally along the axis of differentiated myotubes. It remains to be determined whether DNM2 has a role in this reorganization in muscle and in the positioning of nuclei[15].

In summary, our results represent the first report to our knowledge of a gene mutated in dominant CNM. We identified several missense mutations in the middle domain of DNM2 that result in altered centrosomal localization of DNM2 *in vitro*. Considering the broad range of the cellular mechanisms in which DNM2 is involved, our study opens new avenues for understanding better the pathophysiology of the CNMs.

Note: Supplementary information is available on the Nature Genetics website.

ACKNOWLEDGMENTS

We thank the affected individuals and their families for their participation in this study, J.P. Leroy and J.L. Mandel for continuous support, E. Ralston for comments and suggestions on the manuscript, A. Rouche for assistance with immunohistochemistry and C. Lacroix for providing a DNA sample. This work was supported by the Institut National de la Santé et de la Recherche Médicale, the Centre National de la Recherche Scientifique, the Hôpital Universitaire de Strasbourg, the Collège de France and the Association Française contre les Myopathies. H.L. is member of the German Muscular Dystrophy Network supported by the German Ministry of Education and Research. P.-Y.J. was a recipient of a fellowship from the Swiss Foundation for Research on Muscle Diseases. A.H.B. was supported by a grant from the US National Institutes of Health and the Joshua Frase Foundation. M.B. was the recipient of an Association Française contre les Myopathies fellowship.

COMPETING INTERESTS STATEMENT

The authors declare that they have no competing financial interests.

Published online at http://www.nature.com/naturegenetics/
Reprints and permissions information is available online at http://npg.nature.com/reprintsandpermissions/

1. Spiro, A.J., Shy, G.M. & Gonatas, N.K. *Arch. Neurol.* **14**, 1–14 (1966).
2. Jeannet, P.-Y. *et al. Neurology* **62**, 1484–1490 (2004).
3. Fardeau, M. & Tomé, F.M. in *Myology* 2nd edn. (Engel, A.G., Franzini-Armstrong, C., eds.) 1500–1504 (McGraw-Hill, New York, 1994).
4. Laporte, J., Bedez, F., Bolino, A & Mandel, J.-L. *Hum. Mol. Genet.* **12**, R285–R292 (2003).
5. Cook, T.A., Urrutia, R. & McNiven, M.A. *Proc. Natl. Acad. Sci. USA* **91**, 644–648 (1994).
6. Praefcke, G.J. & McMahon, H.T. *Nat. Rev. Mol. Cell Biol.* **5**, 133–147 (2004).
7. Jones, S.M., Howell, K.E., Henley, J.R., Cao, H. & McNiven, M.A. *Science* **279**, 573–577 (1998).
8. Yoo, J., Jeong, M.J., Cho, H.J., Oh, E.S. & Han, M.Y. *Biochem. Biophys. Res. Commun.* **328**, 424–431 (2005).
9. Orth, J.D. & McNiven, M.A. *Curr. Opin. Cell Biol.* **15**, 31–39 (2003).
10. Thompson, H.M., Cao, H., Chen, J., Euteneuer, U. & McNiven, M.A. *Nat. Cell Biol.* **6**, 335–342 (2004).
11. Züchner, S. *et al. Nat. Genet.* **37**, 289–294 (2005).
12. Smirnova, E., Shurland, D.L., Newman-Smith, E.D., Pishvaee, B. & van der Bliek, A.M. *J. Biol. Chem.* **274**, 14942–14947 (1999).
13. Chen, Y.J., Zhang, P., Egelman, E.H. & Hinshaw, J.E. *Nat. Struct. Mol. Biol.* **11**, 574–575 (2004).
14. Tassin, A.M., Maro, B. & Bornens, M. *J. Cell Biol.* **100**, 35–46 (1985).
15. Reinsch, S. & Gonczy, P. *J. Cell Sci.* **111**, 2283–2295 (1998).

	Distance		θ						
Marker	cM	Mb	0.0	0.01	0.05	0.1	0.2	0.3	0.4
D19S216	20.01	4.9	-4.75	-3.60	-1.93	-1.04	-0.27	0.03	0.10
D19S1034	20.75	6.06	-0.26	0.51	1.10	1.25	1.14	0.79	0.36
D19S884	26.37	8.05	6.20	6.08	5.60	4.97	3.66	2.28	0.95
D19S865	32.39	9.03	4.38	4.29	3.96	3.52	2.60	1.62	0.69
D19S584	34.25	11.06	2.93	2.85	2.53	2.13	1.35	0.68	0.20
D19S226	42.28	14.49	3.98	3.87	3.41	2.83	1.71	0.81	0.26
D19S432	42.28	15.54	5.36	5.24	4.75	4.13	2.92	1.77	0.69
D19S899	45.48	17.09	-0.87	-0.40	0.31	0.59	0.66	0.48	0.23

Supplementary Table 1. Cumulative two-point lod scores for chromosome 19p13 markers.

θ represent recombination fractions. For each marker, the genetic distance is given in centiMorgans according to the Genetic Map index from Marshfield database (http://research.marshfieldclinic.org), and the position in Megabases from the telomere according to the NCBI Map Viewer server (http://www.ncbi.nlm.nih.gov/mapview/).

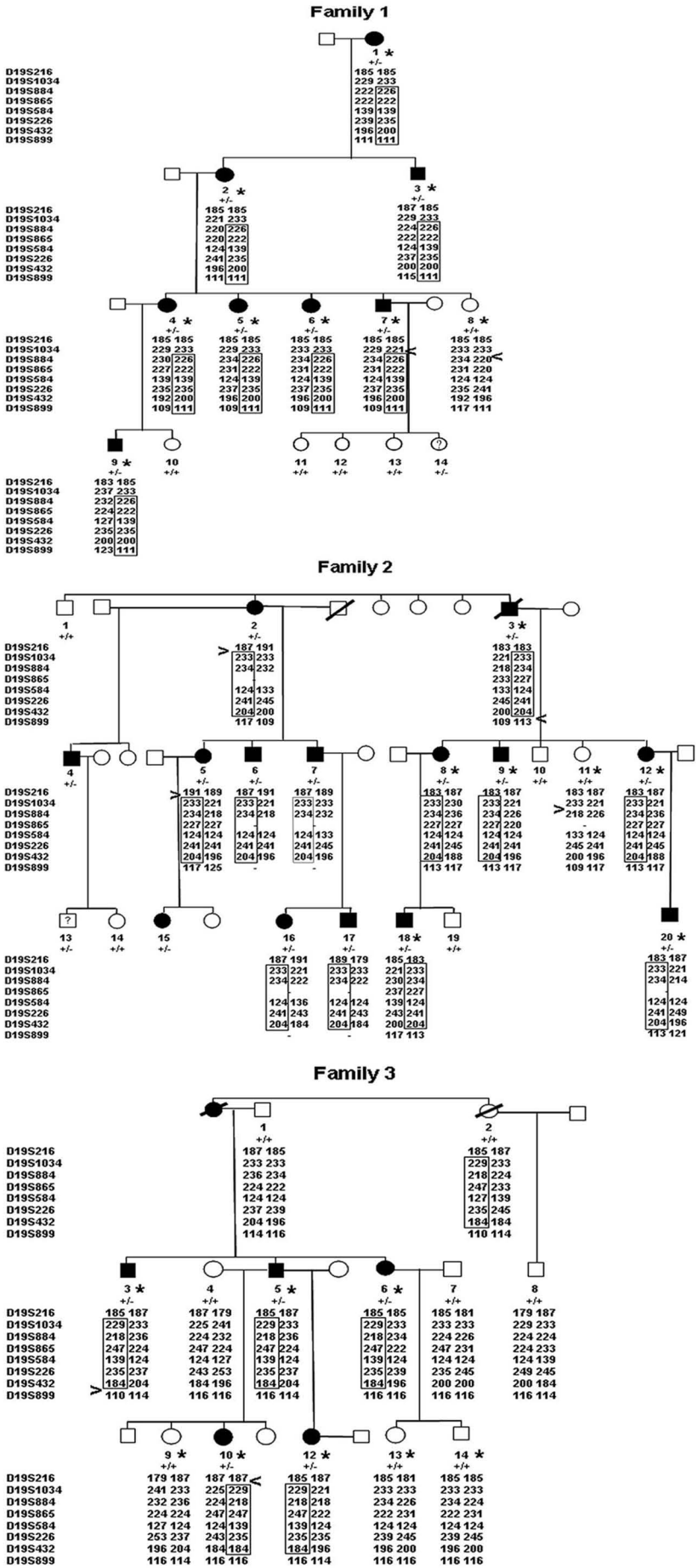

Supplementary Figure 1. Phenotype and haplotype analysis of 3 autosomal dominant CNM families and *DNM2* genotyping.

The phenotype of CNM families is indicated using filled symbols (clinically affected subjects) and open symbols (unaffected subjects). Squares indicate males, circles indicate females and slashed-through symbols indicate deceased subjects. "?" indicates a young subject (3 year-old) with a mild ptosis (Subject 14 in Family 1) and a subject without clinical information (Subject 13 in Family 2). Asterisks show individuals initially included in the genome-wide screening. The haplotypes cosegregating with the disease are boxed for each family. < and > indicate the location of the recombination events. In Family 3, the R369W mutation likely represents a *de novo* event in the affected grand-mother since her unaffected sister was carrier of the disease haplotype but not of the mutation, in contrast to all the other affected members of the family. For the *DNM2* genotyping, +/+ and +/- show homozygous wild type sequence and heterozygous mutated sequence, respectively.

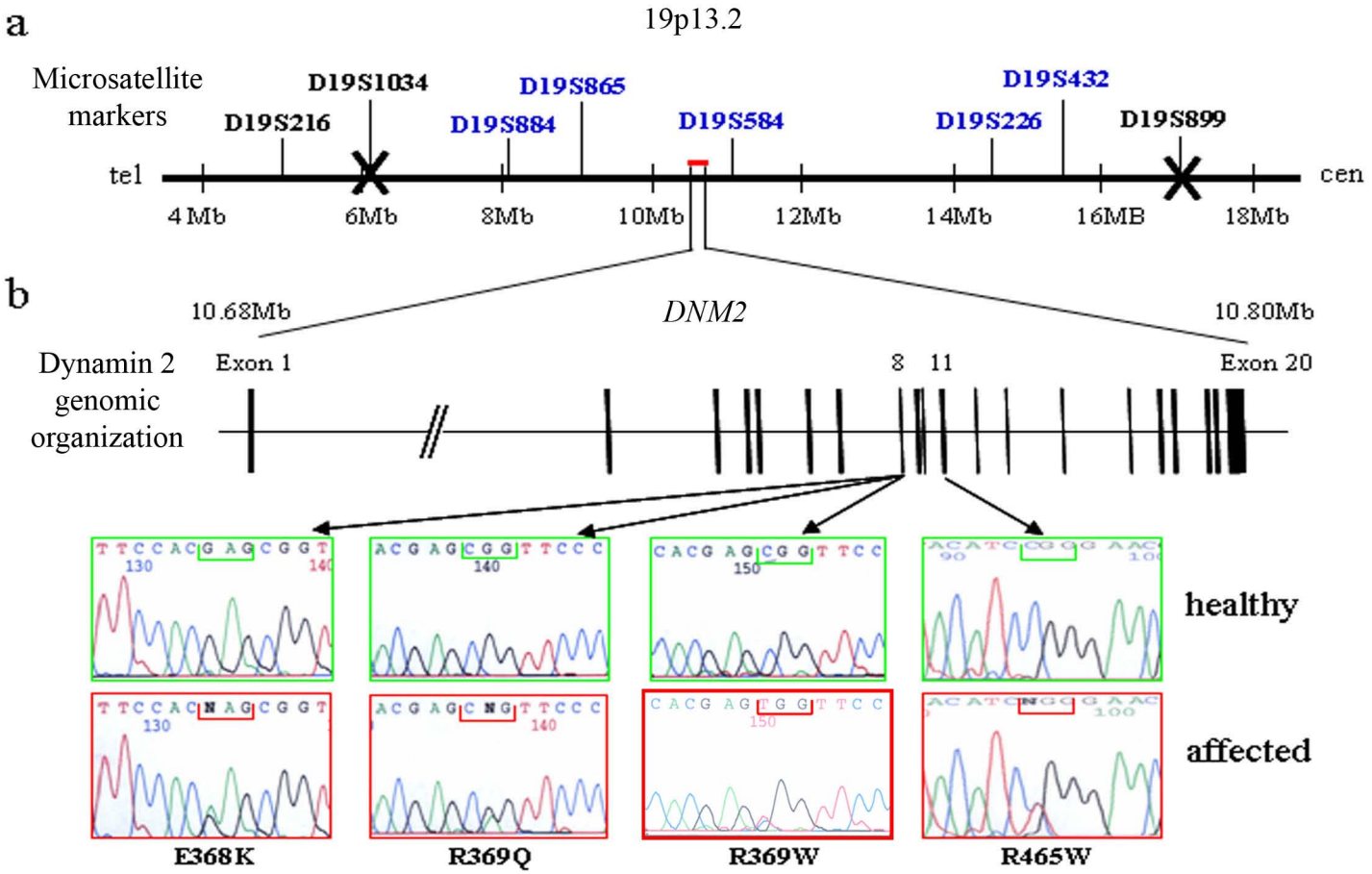

Supplementary Figure 2. Physical map of the CNM locus and *DNM2* mutations.

(**a**) Physical map in the 19p13.2 genomic region and microsatellite markers used for linkage analysis. Linked markers with positive cumulative lod scores for Families 1 to 3 are indicated in blue and recombination events are indicated by a cross. tel: telomere. cen: centromere. (**b**) Genomic organization of *DNM2* consisting of 20 coding exons and electrophoregrams of *DNM2* exons 8 and 11 showing wild type sequence in unaffected subjects and the heterozygous mutations in affected subjects. Heterozygous mutations result in amino-acids changes located to position 368 (G→A that changes glutamic acid to lysine), position 369 (C→T that changes arginine to glutamine and G→A that changes arginine to tryptophane) and position 465 (C→T which changes arginine to tryptophane). (**c**) SSCP profiles of exon 8 and exon 11 and AciI restriction pattern of exon 8. Left: typical profiles obtained by SSCP for mutation E368K in exon 8 and R465W in exon 11 in comparison with PCR products from control subjects. Arrows indicate additional bands in the mutated subjects. Right: typical restriction pattern of exon 8-PCR products from control and mutated subjects, digested by AciI enzyme. Both mutations R369W and R369Q abolish restriction site of AciI and the undigested allele corresponding to the mutant form is identified on agarose gel.

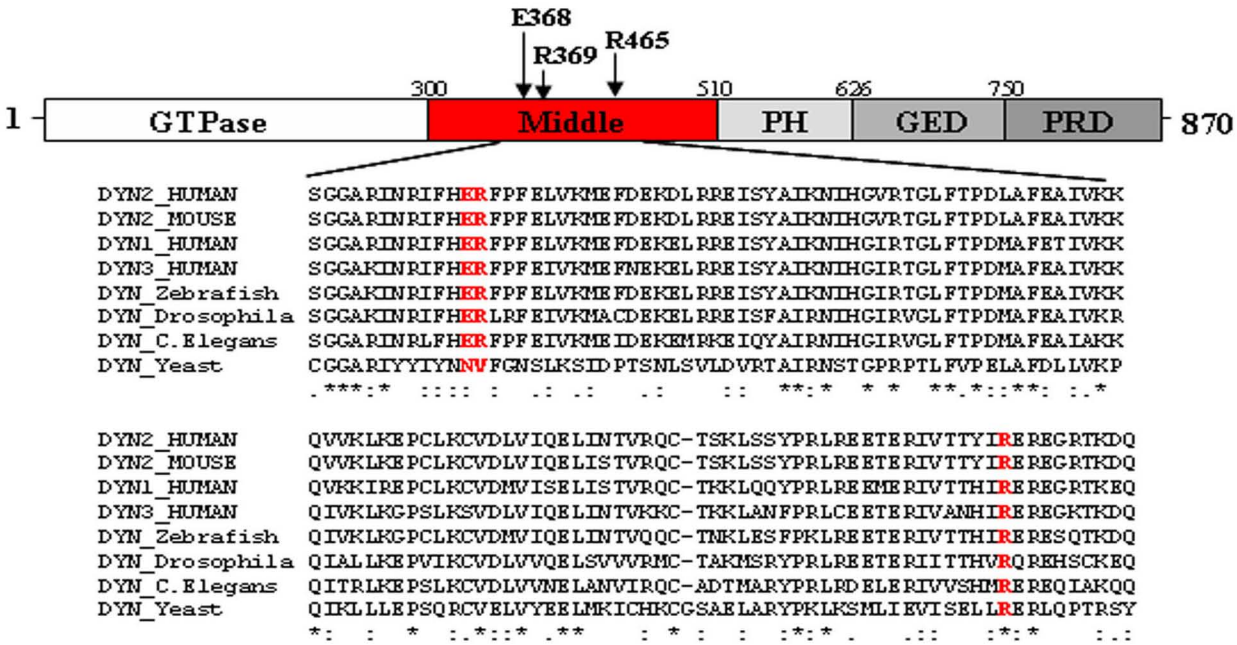

Supplementary Figure 3. Predicted DNM2 structure and multiple protein alignment.

The predicted protein structure includes a tripartite GTPase domain (GTPase), a middle domain (Middle), a Pleckstrin Homology domain (PH), a GTPase effector domain (GED) and a Proline rich domain (PRD). All mutations were detected in 3 amino-acids (368, 369 and 465) located in the middle domain of the DNM2 sequence and affect conserved residues within the human dynamin family and orthologues from different species (indicated in red).

Supplementary Methods

CNM families. For identification of the CNM locus, three large autosomal dominant CNM families were selected: Families 1 and 3 with classical AD CNM form and Family 2 with a milder phenotype associated with diffuse muscle hypertrophy. CNM was diagnosed because several members of these 3 families presented typical clinical pictures of centronuclear myopathy (delayed milestones, muscle weakness, contractures, ptosis, ophtalmoparesis) coexisting with the following histopathological pattern of muscle biopsies: i) centrally located nuclei in >5% of extrafusal fibres, ii) type 1 fibre hypotrophy evidenced through myosin adenosine triphosphatase (ATPase; pH 9.4) staining, and iii) radial arrangement of sarcoplasmic strands around central nuclei on nicotinamide adenosine-tetrazolium reductase staining. Patients were included in the linkage analysis with an affected status only if they present characteristic clinical signs of CNM, with or without biopsy examination. Thus, twenty affected patients with biopsy and six patients without biopsy (patient 7 in Family 1 and patients 5, 12, 16, 17 and 20 in Family 2) were included. In order to avoid inclusion of asymptomatic carriers as healthy in the Lod score calculation, subjects were included as healthy in the analysis only if their muscle biopsy was devoid of morphological abnormalities.

Linkage analysis. Blood samples were obtained after informed consent from eleven families with CNM affected patients and DNA was extracted according to standard procedures. A genome-wide screening was performed on Families 1 and 2 using a 400 microsatellite marker set (Applied Biosystems) at the “National Centre of Genotyping” (Evry, France). Genetic linkage of the disease was performed by analysis of the microsatellite markers D19S216, D19S884, D19S865, D19S226, and D19S899 from genome-wide screening and additional markers D19S1034, D19S584 and D19S432. Polymerase chain reactions (PCR) were carried out with 24 ng DNA. We used the touchdown PCR method, with annealing temperature decreasing from 70 to 60°C in the first 10 cycles, and fixed at 60°C in the final 25 cycles. All PCRs were done using Platinum Taq polymerase (Invitrogen, France) for amplification. PCR products were amplified using forward primers labelled with 6-Fam or Hex fluorochromes, and migrated on an ABI 377 automated sequencer. Data were analyzed by the Genotyper 2.5 software (Applied Biosystems) and haplotypes were constructed. Statistical analysis was performed using the LINKAGE 5.2 package assuming an autosomal dominant inheritance, an equal male and female recombination rate, a disease gene frequency of 0.0001, and a

penetrance of 0.9. Cumulative lod scores for Families 1 to 3 were calculated with isoallelic frequencies.

***DNM2* sequencing.** Six AD families (Families 5, 6, 7, 8, 9 and 11) and two families with sporadic cases (Families 4 and 10) were added to Families 1, 2 and 3 for the screening of the *DNM2* gene mutations. The genomic sequence of the human dynamin 2 was used to design intronic primers to amplify the 20 exons. Primer sequences are available on request. Polymerase chain reactions (PCR) were carried out with 100 ng DNA. We used the touchdown PCR method, with annealing temperature decreasing from 70 to 60°C in the first 10 cycles, and fixed at 60°C in the final 30 cycles. All PCRs were done using Platinum Taq polymerase (Invitrogen, France) for amplification. Purified PCR products were analyzed in the both strands by uni-directional sequencing with ABI PRISM BigDye Terminator cycle sequencing ready reactions kit 3.1 and run on a 377 Genetic Analyzer (Applied Biosystems). Sequences were analyzed using Sequencing Analysis 3.4 software (Applied Biosystems). All detected mutations were analyzed at least twice by sequencing in both directions.

Validation of DNM2 mutations. Absence of mutations was checked in 150 healthy Caucasian control subjects of European origin. Controls were screened for mutations by Single Strand Conformation Polymorphism (SSCP) for mutations R465W and E368K or restriction enzyme digestion using AciI for mutations R369W and R369Q. For SSCP, exon 8- and exon 11-PCR products were denatured 5 min at 94°C. Samples were then submitted to electrophoresis on non-denaturing 10% polyacrylamide gels at 20°C for exon 8 or 25°C for exon 11, and subsequently analyzed through silver nitrate staining. For restriction pattern analysis, exon 8-PCR products were digested overnight at 37°C using 2 U of AciI restriction enzyme (New England, BioLabs inc.). Digestion products were then submitted to electrophoresis on 2% agarose gels.

Cell culture, constructs and transfection. Fibroblasts were cultured from skin biopsies of a 33 year-old patient from Family 1 and a 28 year-old patient from Family 6 in Dulbecco's modified Eagle's medium (DMEM) supplemented with 10% foetal calf serum (FCS) in a 5% CO_2 incubator at 37°C. For transfection studies, skin fibroblasts from two healthy adult subjects were used as controls. The open reading frame of wild-type DNM2 and of two mutants (C1393T and C1105T corresponding to amino acid changes R465W and R369W, respectively) were generated by RT-PCR from lymphocyte mRNA and inserted in frame with

the Green Fluorescent Protein (GFP) in pGFP-NT-TOPO-TA vector (Invitrogen, France). Human fibroblasts were seeded in 35 mm diameter plates and transfected at 50% confluency using Lipofectamine reagent following manufacturer's instructions (Invitrogen, France). Briefly, 1 μg plasmid and 10 μl Lipofectamine were mixed for 30 min in OptiMEM-1 culture medium (Invitrogen) and then added to cells for 4 hours at 37°C. This transfection medium was then replaced by DMEM-10% FCS for 2 days before γ-tubulin immunolabelling.

Immunocytochemistry. Fibroblasts were washed in PBS and then fixed 20 min at -20°C in acetone before immunolabelling. Non specific sites were blocked in PBS with 5% FCS and 0.01% Triton X-100 for 90 min and incubated overnight with the mouse monoclonal antibody C11 directed against human γ-tubulin (Santa Cruz Biotechnology) or mouse monoclonal antibody against human α-tubulin (Sigma Aldrich) diluted at 1:200 in blocking buffer. After washing, immunostaining was revealed by incubation for 2 hours with an anti-mouse antibody-Cy3 (Jackson ImmunoResearch) diluted at 1:200 in blocking buffer. For double immunolabelling, primary antibodies against human dynamin 2 (C18-goat antibody, Santa Cruz Biotechnology) and against γ-tubulin were mixed at 1:200 in blocking buffer. Immunostaining was revealed using a mixture of rabbit anti-goat-Cy3 and sheep anti-mouse-FITC (Chemicon International) at 1:400 in blocking buffer. Labelled cells were visualized by fluorescence microscopy (Axiophot system Zeiss, Germany) coupled with a CCD camera and images were acquired using the Metaview software (Universal Imaging, USA).

Western-blotting. Twenty μg of protein from control and CNM-fibroblasts in loading buffer (50 mM Tris-HCl, 2% SDS, 10% glycerol, 1% β-mercaptoethanol and bromophenol blue) were submitted to electrophoresis on a 10% SDS-PAGE gel and then transferred onto polyvinylidene difluoride (PVDF) membranes (Invitrogen). Non specific sites were blocked for 2 hours at room temperature in PBS with 5% nonfat dry milk and 0.1% Triton X-100. Incubation with primary antibody was performed overnight at 4°C for antibody against DNM2 (C18-goat polyclonal antibody raised against a peptide mapping at the carboxy terminus of DNM2, Santa Cruz Biotechnology, 1:200) or 1 hour at room temperature for antibody against α-tubulin (mouse monoclonal antibody from Sigma Aldrich, 1:1000) diluted in the blocking buffer. After washing, membranes were incubated 2 hours at room temperature with Horseradish Peroxidase (HRP)-conjugated secondary antibodies (anti-goat-HRP from Jackson ImmunoResearch and anti-mouse-HRP from Dako) diluted at 1:2000 in blocking

buffer. Detection was performed using the Supersignal West Pico Chemiluminescent kit (Pierce).

Accession numbers. Human DNM2 mRNA GenBank NM_001005360. Human DNM2 genomic sequence GenBank NT_011295. Human DNM2 protein Genbank P50570. Mouse DNM2 protein Genbank P39054. Human DNM1 protein Genbank Q05193. Human DNM3 protein Genbank Q9UQ16. Zebrafish DNM protein Genbank AAH65325. Drosophila DNM protein Genbank P27619. Caenorhabditis elegans DNM protein Genbank P39055. Yeast DNM protein Genbank P54861.